IAC-15-A6.9.9

A COVARIANCE ANALYSIS TO OPTIMIZE THE OPTICAL FOLLOW-UP STRATEGIES

Emiliano Cordelli
Astronomical Institute University of Bern (AIUB), Switzerland, emiliano.cordelli@aiub.unibe.ch

Dr. Alessandro Vananti
Astronomical Institute University of Bern (AIUB), Switzerland, alessandro.vananti@aiub.unibe.ch
Prof. Thomas Schildknecht
Astronomical Institute University of Bern (AIUB) / SwissSpace Association, Switzerland,
thomas.schildknecht@aiub.unibe.ch

The Astronomical Institute of the University of Bern (AIUB) is conducting several search campaigns for space debris using optical sensors. The debris objects are discovered during systematic survey observations. In general, the result of a discovery consists in only a short observation arc, or tracklet, which is used to perform a first orbit determination in order to be able to observe the object again in subsequent follow-up observations. The additional observations are used in the orbit improvement process to obtain accurate orbits to be included in a catalogue. In order to obtain the most accurate orbit within the time available it is necessary to optimize the follow-up observations strategy.

In this paper an in-depth study, using simulations and covariance analysis, is performed to identify the optimal sequence of follow-up observations to obtain the most accurate orbit propagation to be used for the space debris catalogue maintenance. The main factors that determine the accuracy of the results of an orbit determination/improvement process are: tracklet length, number of observations, type of orbit, astrometric error of the measurements, time interval between tracklets, and the relative position of the object along its orbit with respect to the observing station. The main aim of the covariance analysis is to optimize the follow-up strategy as a function of the object-observer geometry, the interval between follow-up observations and the shape of the orbit. This analysis can be applied to every orbital regime but particular attention was dedicated to geostationary, Molniya, and geostationary transfer orbits. Finally the case with more than two follow-up observations and the influence of a second observing station are also analyzed.

I. INTRODUCTION

At the moment, in the space around the Earth, there are more than 29000 objects with a diameter bigger than 10 cm, and more than 670000 objects bigger than 1 cm; furthermore, according to estimates there are more than 170 million objects bigger than 1 mm[1]. Among all these objects, only about 1400 are active satellites, all the rest is space debris.

Space debris constitutes a serious problem for space missions, both, manned and robotic. Because of the high velocities of the debris particles, the present shields are able to protect spacecraft only from debris whose size is smaller than 1 centimetre[2].

The Astronomical Institute of the Univerity of Bern (AIUB) is also involved in the space debris field of research. In particular, the AIUB, using its telescopes, is contributing to answer the most common questions related to space debris like: how many debris objects are there? What are the most populated regions? What are they made of? And how will this population evolve in future? To answer these questions the most common approach consists of three main steps: the first is the discovery of the objects[3], the second is the orbit

determination[4] and the third is the characterization of the objects[5].

The discovery of the objects is performed by scanning certain regions of the sky chosen in a way to ensure that an object is observed several times during the same night[6]. The orbit determination is performed by planning regular observations of the object of interest, these additional series of observations are usually called follow-up observations. Due to the huge amount of space debris and to the limitations of the telescopes, it is necessary to optimize the use of the time available for observations.

This paper will describe a method, based on the analysis of the covariance matrix, to understand how the observations should be distributed to minimize the uncertainties of the estimated orbital elements in order to maximize the accuracy of the predicted positions of the object. In the first part of the paper we describe the reasons that brought us to use the covariance matrix for this study and we will show the results obtained on a relatively simple scenario to highlight the effects of the main parameters on the results. Then the covariance study is performed on some typical observation scenarios. Finally, we will present the results obtained

from the application of this study in the case of two observers and in the case of more than two series of observations.

II. THEORY

Depending on the number of objects to observe in the catalogue, the survey strategy and also the performance of the software used to extract the measurements from an image, the number of observations per night per object is not constant among the various observatories. To carry out this study we chose the number of observations per object accordingly to what is provided by the AIUB observatory at the end of an observation night. Using the tools available at the AIUB is not unusual to have an average of two standard tracklets per observed object at the end of an observation night. A tracklet is the result of a series of images acquired during a survey campaign or during a follow-up of an already catalogued object. We assume that a standard tracklet is consisting of e.g. 7 images, each one of them contains a triplet of data: a pair of angular measurements, one in Right Ascension (RA) and one in Declination (DE); and the time epoch when the measurements were collected.

These series of observations are then used to determine/improve the orbit of the object by mean of a Least Squares adjustment (LSQ). The aim of this study is to analyse the output covariance of a LSQ process to understand how the relative geometry between observer and target object influences the accuracy of the estimated parameters. The covariance matrix was chosen as the evaluation criterion because, as one can see from Eq. [1], it contains the uncertainties of the estimated parameters as a function of the partial derivatives of the observations w.r.t. them. These partial derivatives are functions of the geometric relation between observer and observed object.

$$P = m^2 [A^T W A]^{-1} \qquad [1]$$

in which:

$$A = \frac{dobs_i}{dX_0} \qquad [2]$$

where:
- P is the covariance matrix,
- m is the a posteriori error for unit weight,
- A is the first design matrix,
- W is the weight matrix,
- $obs_i = [RA_i, DE_i]$ are the ith angular measurements, respectively Right Ascension and Declination, where $i = 1, \dots, n$ and n is the number of observations,

- $X_0 = [a, e, i, \Omega, \omega, u_0]$ are the orbital parameters to be estimated, namely semi-major axis, eccentricity, inclination, Right Ascension of Ascending Node (RAAN), argument of perigee and argument of latitude at the osculating time T_{osc}.

The argument of latitude was chosen instead of the classical perigee passing time (T_0) because for circular orbit the perigee is not defined, then also T_0 is not defined anymore. Hence, exploiting the definition of osculating elements[7], the user can set up an arbitrary osculating time (T_{osc}), with a certain ω and true anomaly at this time (ν_0), and solve the LSQ adjustment at this epoch.

Another important information is contained within the correlation indices which can be retrieved from the covariance matrix as shown in Eq. (3). These indices are useful because they tell us how strong any two parameters are correlated.

$$\rho_{ij} = \frac{\sigma_{ij}}{\sigma_i \sigma_j} \qquad [3]$$

where:
- $-1 \leq \rho \leq 1$ is the correlation index,
- σ_{ij} is the covariance of the elements i and j,
- σ_i and σ_j are the standard deviation of the elements i and j.

III. METHOD

The main aim of this study is to understand how the relative object-observer geometry influences the accuracy of the estimated parameters. The first results which will be presented are based on a limited number of observations, in particular only two tracklets are used, each one is made by 7 triplets of measurements (i.e. RA, DE and time epoch). During all simulations the time interval between the measurements within a tracklet is kept constant to 30 seconds. The simulations are performed in order to cover all possible combinations of tracklet positions in the orbit. To do so, the first LSQ adjustment is performed positioning the first tracklet on the orbit perigee and the time interval between first and second tracklet is increased from 10 sec to two orbital revolutions; then, the same procedure is repeated positioning in each run the first tracklet slightly forward along the orbit. During the simulations, the position of the observer is kept constant for the different 1st tracklet positions while for the 2nd tracklet, the position of the observer is rotated accordingly with the time interval between tracklets and Earth's angular velocity. For each couple of tracklets the last iteration of a LSQ adjustment is simulated and from the relative

IAC-15-A6.9.9

covariance matrix the square root of the terms in the main diagonal and the correlation coefficients are stored. Since we are not interested in LSQ performances the correct orbital elements are given as input to the LSQ. It is possible to do this simplification because being a non-linear LSQ, the only requirement to find the minimum is that the initial value of the estimated parameters should be near to the global minimum values to converge to the correct solution[8].

This paper will also show the results obtained from the analysis of two particulars scenarios: in the first, two observers are used, while in the second three tracklets from a single observer are used. In the case of two observers we assumed that they are able to observe the object precisely at the same time. To do this experiment we kept the same procedure as shown before. While in the case of three tracklets, with a single observer, the procedure was slightly modified in order to keep fix the time distance between the 1st and the 2nd tracklet while we let vary the time distance between 2nd and 3rd tracklet.

The procedure just described was repeated for different kinds of orbit and different positions of the observer in order to understand how all these factors influence the accuracy of the estimated parameters.

IV. RESULTS

IV.I First results

In order to easily understand the results and the contribution of each parameter on them, the simulation are performed first on a simple scenario. As "standard" orbit a geosynchronous eccentric orbit is used, its orbital elements are respectively: $a = 42164.173$ km, $e = 0.5$, $i = 0.1°$, $\Omega = \omega = 0°$ and T_{osc} coincides with the time of first observation. While as "standard" observer an equatorial observer on the Greenwich meridian is used. The simulations are then repeated each time modifying one parameter. First the influence of the observer position is evaluated and then also the effects of the orbital parameters are analyzed; the results of these simulations are shown in the following paragraph.

Finally, it is important to note that being a geometrical study the real orientation of the Earth in the space is neglected. To better understand the results we set up the orbits so that their line of nodes/apsides are coincident with the x-axis of the generic inertial system; and the Greenwich meridian is also aligned with the same axis at time $t = 0$.

The results obtained for the just described scenario are displayed from Fig. 1.A to Fig. 1.F. Each point of the figures shows the logarithm, with base ten, of the square root of the uncertainty of the estimated parameter as a function of the tracklets positions. In particular, the position of the 1st tracklet along the orbit can be read on the y-axis, while the position of the 2nd is displayed on the x-axis. Both positions are expressed in terms of true

anomaly.
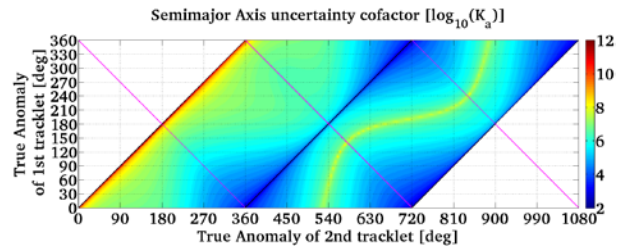
Fig. 1.A Semi-major axis uncertainty map.
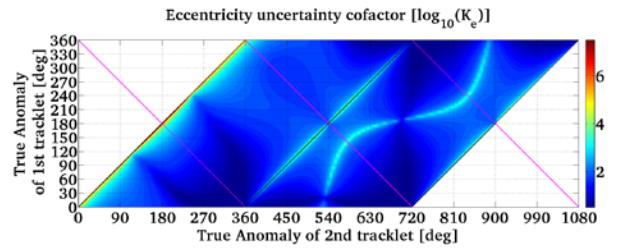
Fig. 1.B Eccentricity uncertainty map.
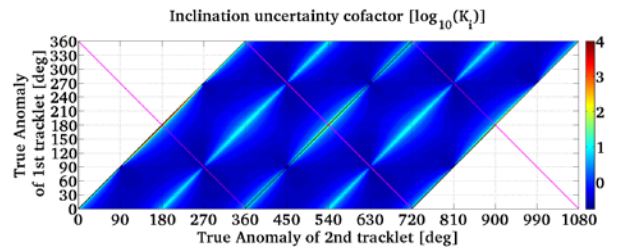
Fig. 1.C Inclination uncertainty map.
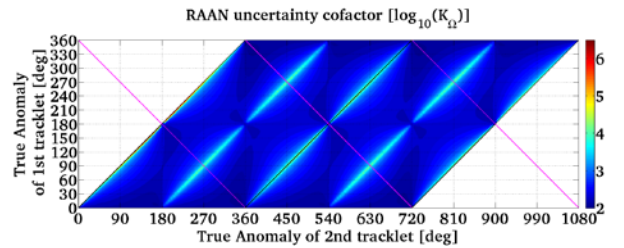
Fig. 1.D RAAN uncertainty map.
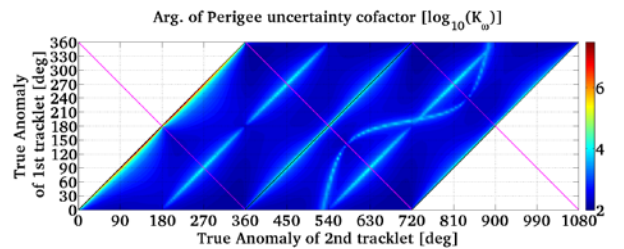
Fig. 1.E Argument of perigee uncertainty map.
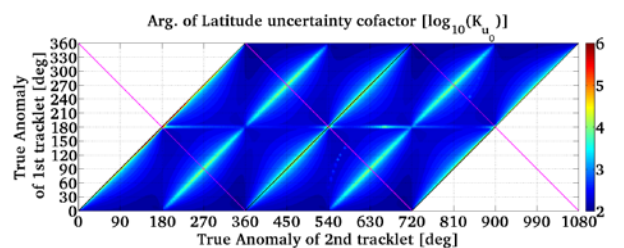
Fig. 1.F Argument of latitude uncertainty map.

From the figures just shown (Fig. 1.A to Fig. 1.F) it is possible to notice some important characteristics: the first is given by the fact that for the semi-major axis, for the eccentricity and for the argument of perigee the features visible in the first orbital revolution are different from those visible in the second, this is a consequence of the time dependency of the partial derivatives of the observation w.r.t. the semi-major axis. The second is that for the same elements an S-shaped high uncertainty area is visible when the time distance between the tracklets is more than one orbital period; more precisely the S-area is occurring when the time distance between tracklets is 1.5 orbital periods. Comparing the S-area of the eccentricity and the argument of perigee with that of the semi-major axis it is easy to notice how the first two show some interruptions while the third is continuous. Being this an elliptical orbit and the tracklets are acquired with a constant time separations between observations, it is obvious that the arc of orbit covered by the tracklet depends on the position of the tracklet; furthermore, for the same reason, also the distance between single observations is not constant. This effect provides information regarding the eccentricity of the orbit and the argument of perigee. If one pays attention the interruptions for the eccentricity are occurring when the 1st tracklet is at the apogee while the 2nd is at the perigee and vice versa. This tracklets combination maximizes the ratio between the lengths of the arcs covered by the tracklets. The interruptions for the argument of perigee are occurring when the tracklets are symmetric w.r.t. the line of the apsides. In this configuration two tracklets of the same length are used, and the distances between the observations within the tracklet are first increasing then decreasing (or vice versa) in the same way. This tells us if the apogee or the perigee is precisely in the middle of the arc defined by the two tracklets.

Fig. 1.C and Fig. 1.D show the uncertainty maps for i and Ω which are characterized by one main feature of high uncertainty values which includes all the positions with a difference in time of one (or more) orbital period and which are separated by 180° in true anomaly. These two position vectors are parallel and then it is not possible to define the orbital plane. These features present some interruptions that, for the inclination, are occurring when the tracklets are at the maximum distance from the line of the nodes; while, for the RAAN, the interruptions occur when the tracklets are on the line of the nodes.

For completeness Fig. 1.F shows the uncertainty map for the argument of latitude at time T_{osc} (u_0). The results for this parameter will not be shown anymore on this paper because our interest is mainly focused on the geometric parameters.

Finally, it is important to highlight two particular regions on the uncertainty maps: the first, identified by the black diagonal line, whose extremes have coordinates $[v_2 = 360, v_1 = 0]$, $[v_2 = 720, v_1 = 360]$, defines all tracklets whose positions are separated by one (or more) orbital period in time. The second, identified by the magenta line, whose extremes have coordinates $[v_2 = 360, v_1 = 360]$, $[v_2 = 720, v_1 = 0]$, defines all tracklets whose positions are symmetric to the lines of the apsides. Of course all the lines parallel to the before mentioned ones, with a distance multiple of 360°, have the same meaning.

Influence of observer position

To study the influence of the observer position the results and the scenario described in the previous paragraph are taken as reference then the simulations are repeated changing the position of the observer on the Earth's surface. In particular, first the case with an observer on the Greenwich meridian with a latitude of 50° North is analysed; then the position of the equatorial observer is displaced by 50 degree in longitude w.r.t. the reference position.

Fig 2.A, Fig 2.B and Fig 2.C show the uncertainty maps for a, i and ω obtained with the reference orbit and the observer displaced in latitude by 50°.
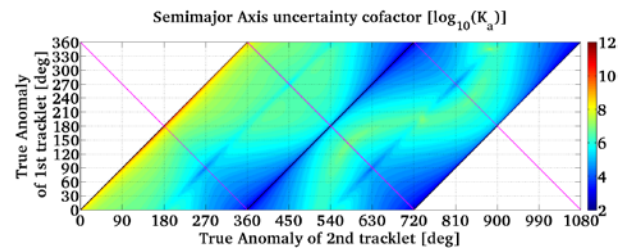
Fig 2.A Semi-major axis uncertainty map with a latitude displaced observer.
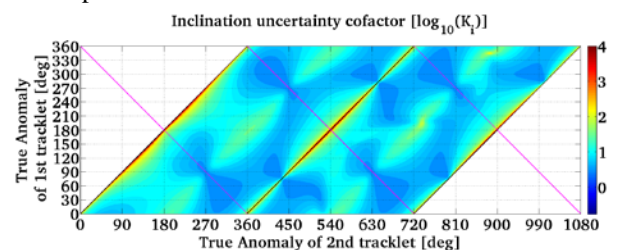
Fig 2.B Inclination uncertainty map with a latitude displaced observer.
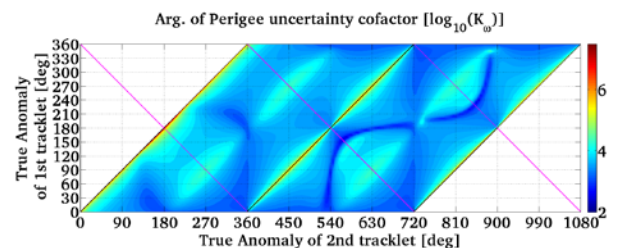
Fig 2.C Argument of perigee uncertainty map with a latitude displaced observer.

Comparing the results in Fig 2.A, Fig 2.B and Fig 2.C respectively with those in Fig. 1.A, Fig. 1.C and Fig. 1.E one has to take into account that the first ones are obtained with an observer always outside the orbital plane while the seconds with one always inside the orbital plane. This distinction is very important because having only angular measurements in principle is not possible to directly estimate distances. Being outside the orbital plane, knowing the position of the observer and the direction of the observations, one is able to estimate the distance of the object from the observer. This effect is clearly visible in the semi-major axis uncertainty map where the intensity of the S-area is strongly reduced in the case of latitude displaced observer; the same effect is noticeable for the map w.r.t. the eccentricity. In Fig 2.A also a new feature is visible: a diagonal line with low uncertainty values when $v_2 - v_1 = 180°$. This effect can be explained by the fact that an orbit is a section of a cone; in fact, observing the orbit from the apex of the cone (or from a circular section of the cone) and being able to estimate distances, it is easier to determine semi-major axis and eccentricity.

Comparing now the maps for the inclination (respectively Fig. 1.C and Fig 2.B), one can see that the main features are kept, but there is a reduction of the sharpness of the high uncertainty area for tracklets separated by 180° of true anomaly and the average uncertainty remarkably increased. This is well understandable because the inclination is determined measuring the distance of the object from the equatorial plane; having a relatively small distance, given by the inclination of 0.1°, this can be better measured if the observer is inside the orbital plane.

One interesting result can be seen analysing the maps related to the argument of perigee. Looking at Fig. 1.E is possible to see how the classical high uncertainty S-shaped area is present together with a diagonal high uncertainty area for tracklet separated by 180° in true anomaly. This second feature is characteristic of Ω but is present also on ω because of the small inclination value. For $i \to 0$ it is difficult to define the line of the nodes and being the argument of perigee defined w.r.t. this line all the uncertainties of Ω are transferred to ω (and also to u_0). Comparing these features with those visible in Fig 2.C, it is easy to notice how the S-area is still present but in this case it is a low uncertainty area. This can be explained by the fact that, looking from outside the orbital plane, the improvement given by the capability to estimate distances will produce a better determination of a and e with a consequent decorrelation of them from ω.

The simulations were repeated also in the case with a longitude displaced observer with the same almost equatorial orbit. Like for the reference scenario also in this case, the observer is always within the orbital plane and no significant effects can be seen.

In conclusion, is it better to observe within or outside the orbital plane? There is not a unique answer to this question in fact: the observer inside the orbital plane gains more information about the orientation of the orbital plane in the space, amplifying the effect given by the distance of the observations from the line of the nodes and reducing the average uncertainty values. Vice versa, observing from outside the orbital plane allows the estimation of the distances which reduces the average error on a, strongly reduces the S-area for a, e and ω, and helps to decorrelate the argument of perigee from the eccentricity and the semi-major axis.

Influence of orbital parameters
Once the main features in the results were studied, the analysis was repeated varying the orbital parameter of the reference orbit in order to understand their influences.

First, the influence of u_0 was studied: modifying u_0 is equivalent to change the osculating time, this means to solve the orbit determination problem for positions of the object in a different place of the orbit. This analysis showed that the modification on this parameter affects only the map of the argument of latitude while is not influencing the other geometric parameters.

The argument of perigee describes the orientation of the orbit within the orbital plane, changing it, means to change the intersection points of the orbit with the equatorial plane producing only a translation of the minimum horizontal lines seen in the maps of the inclination and of the RAAN.

Changing the position of the line of the nodes (Ω) produces the same effect of a longitude displacement of the observer changing the relative position of the observer w.r.t. the orbital plane. In particular the observer will be inside or outside the orbital plane for different time distances between the tracklets reducing the strength of the S-area for a and e if the observer will be more outside the orbital plane and influencing the low uncertainty area for i and Ω.

The main effect related to the inclination is given when i tends to 0. If $i = 0 \Rightarrow \Omega$ is not defined. The main effect of this singularity is visible in the map of ω because being defined since the line of the nodes it will present the characteristics features of Ω. Additionally the closer is i to 0 the fainter will be the S-area for ω. Finally being $u_0 = \omega + v_0$ the main features of Ω are consequently transferred also to the argument of latitude.

The eccentricity is the main responsible for the S-area, in particular if e grows the S tends to have the shape of two hyperbolas, while if e decreases the S

tends to become a diagonal line for tracklets separated by 180° in true anomaly.

The last interesting effects are given by the variations of the semi-major axis which are related to the Earth's parallax, the length of the arc covered by the tracklet and the ratio between Earth's rotation period and orbital period. Increasing the semi-major axis means augmenting the distance of the object from the observer. This produces a general rise of the average uncertainty values especially for a and e. If the object is enough distant from the Earth the effect given by the Earth's parallax and those given by the observer outside the orbital plane are strongly reduced with results similar to those obtained for an observer always within the orbital plane. Furthermore, the time interval between observations within a tracklet is kept constant during the simulations; this leads to a decrease of the length of the arc of orbit covered by a tracklet producing a loss of information for a, e and ω. The ratio between the orbital period and the Earth's rotation is important because it will determine when an observer is within or outside the orbital plane. As seen before this is important for the high uncertainty S-shaped area.

IV.II Application on real orbits

Once the effects of each single parameter and those related to the position of the observer are known, the next step is to apply this method to a real scenario characterized by a real orbit with a real observer. The following paragraphs will show the results obtained for three orbits which are largely populated by satellites and by space debris: the geostationary orbit (GEO), the geostationary transfer orbit (GTO) and Molniya orbit characterized by high eccentricity and inclination.

GEO

For this simulation the following orbital parameters are used: $a = 42164.173$ km, $e = 0.0005, i = 0.1°$, $\Omega = 270°, \omega = 0°$ and $T_{osc} = 1^{st}$ observation. For the observer position the Zimmerwald observatory is used whose geodetic coordinates are: 46.8772° North, 7.4652° East and 951.2 m altitude. A maximum distance of 2 orbital revolutions between the two tracklets is allowed.
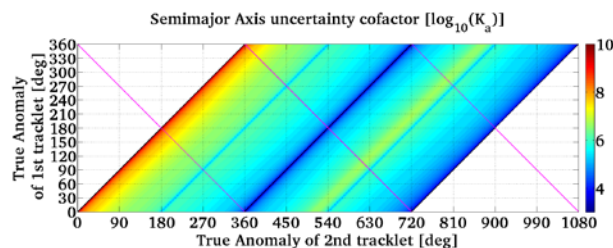
Fig. 3.A Semi-major axis uncertainty map for GEO object.
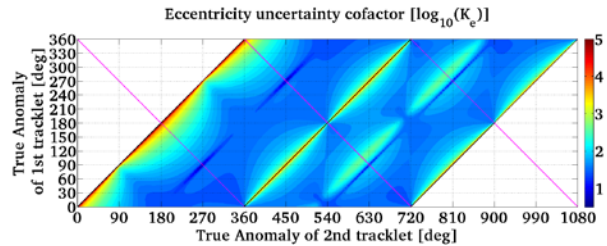
Fig. 3.B Eccentricity uncertainty map for GEO object.
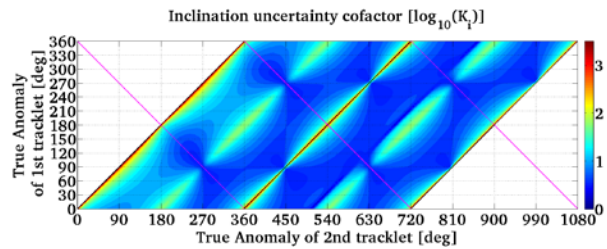
Fig. 3.C Inclination uncertainty map for GEO object.
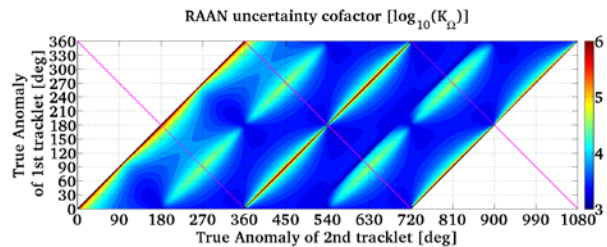
Fig. 3.D RAAN uncertainty map for GEO object.
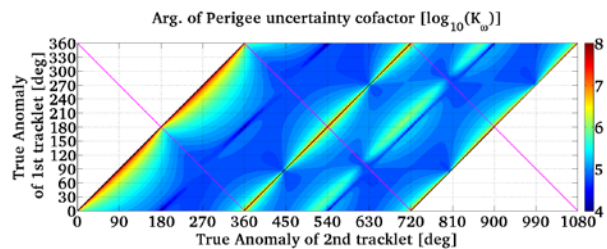
Fig. 3.E Argument of perigee uncertainty map for GEO object.
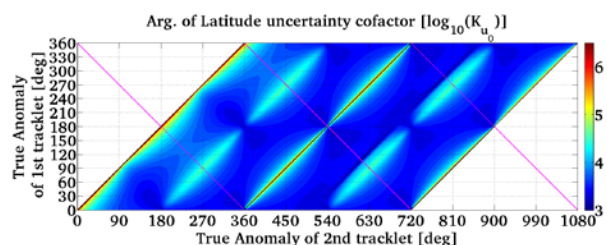
Fig. 3.F Argument of latitude uncertainty map for GEO object.

As one can see from Fig. 3.A, Fig. 3.B and Fig. 3.E, being this a circular orbit, the S-area is now a diagonal line which is not yet precisely coincident with that of 180° angular distance between tracklets because of the effect of the time dependency. The diagonal line of tracklet positions which are separated by 180° in true anomaly is due to the fact that the observer is always outside the orbital plane. Looking at the uncertainty

map for i and Ω (respectively Fig. 3.C and Fig. 3.D), the high-uncertainty diagonal lines for tracklets separated by 180° and 360° in true anomaly are clearly visible. It is interesting to notice that the 180° tracklets separation, although it is not the best configuration of observation for i and Ω, shows lower uncertainty values than the 360° tracklets separation due to the different geometry condition given by the observer position on the Earth's surface. Other consequences of the small eccentricity values can be observed in the average high uncertainties for the argument of perigee. In this case, despite the small inclination value, the argument of perigee keeps its features while the uncertainties of Ω are directly transferred to u_0 which is completely correlated with it.

GTO

For this simulation the same scenario as described before is used changing only the orbital parameters of the orbit; in particular: $a = 24409.4$ km, $e = 0.7287$, $i = 6°$, $\Omega = 226°, \omega = 0°$.
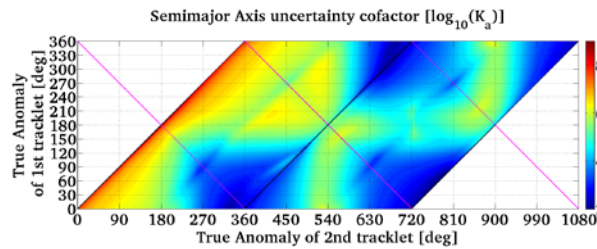
Fig. 4.A Semi-major axis uncertainty map for GTO object.
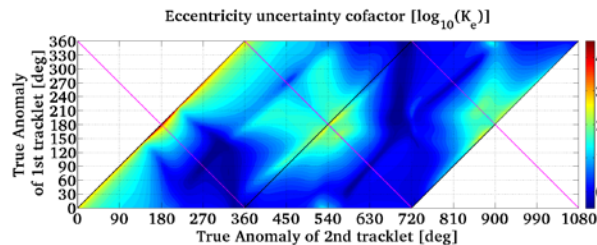
Fig. 4.B Eccentricity uncertainty map for GTO object.
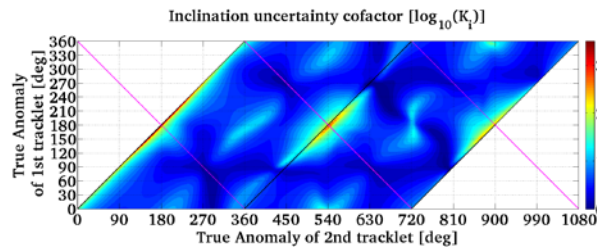
Fig. 4.C Inclination uncertainty map for GTO object.
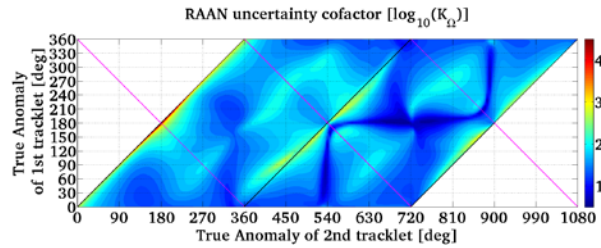
Fig. 4.D RAAN uncertainty map for GTO object.
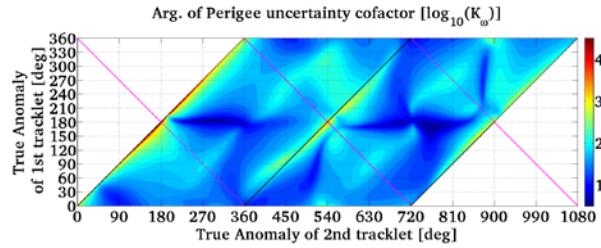
Fig. 4.E Argument of perigee uncertainty map for GTO object.

Although the results shown from Fig. 4.A to Fig. 4.E are a bit more difficult to interpret, it is still possible to recognize some main features. From Fig. 4.A and Fig. 4.B it is easy to see how the S-area is strongly reduced by the fact that the observer is always outside the orbital plane and the orbital period with the Earth's rotation period are not commensurable. In both maps the diagonal line for positions separated by 180°, characteristic of an observer outside the orbital plane, is also present. In Fig. 4.E is possible to see how the S-area is now a minimum uncertainty area due again to the observer position. From Fig. 4.C and Fig. 4.D it is possible to see how the main diagonal features from tracklet separated by 180°, despite strongly reduced, are still presents. Especially for the inclination the highest uncertainty values are visible for tracklets close to the apogee; this is probably given by the sum of the effects due to the high eccentricity of the orbit and the fact that the line of the nodes coincides with the line of the apsides. This configuration is then characterized by the shortest tracklets along the orbit close to the line of the nodes. In the inclination map it is also possible to see two horizontal lines of minimum uncertainty values, respectively for $v_1 = 90°$ or 270°. Knowing that $\omega = 0$, these regions coincide with the tracklets whose positions are at the maximum angular distance from the line of the nodes. Finally, if one looks at the map of Ω, will notice the similarities with that of ω; this is due to the relatively small inclination value which leads to a high correlation of these two parameters.

Molniya

For this simulation the same scenario as described before is used changing only the orbital parameters of the orbit; in particular: $a = 26561.765$ km, $e = 0.7$, $i = 63.4°$, $\Omega = 278°, \omega = 270°$.
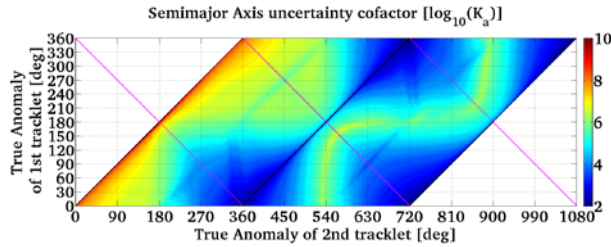
Fig. 5.A Semi-major axis uncertainty map for Molniya object.
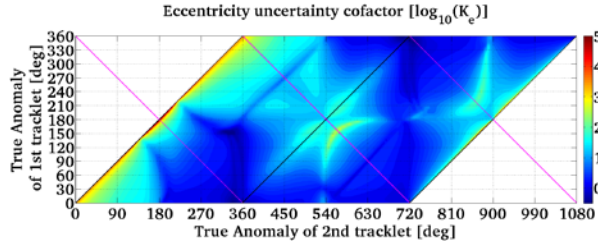
Fig. 5.B Eccentricity uncertainty map for Molniya object.
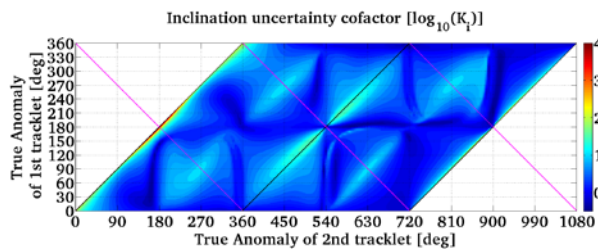
Fig. 5.C Inclination uncertainty map for Molniya object.
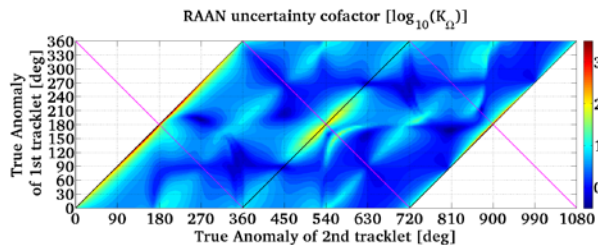
Fig. 5.D RAAN uncertainty map for Molniya object.
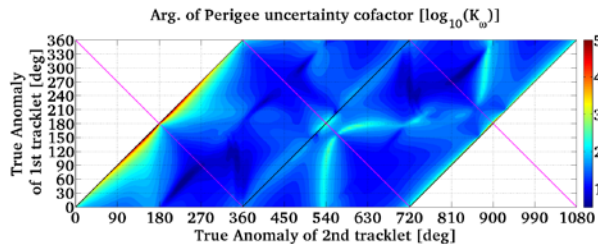
Fig. 5.E Argument of perigee uncertainty map for Molniya object.

As usual, also the results for the Molniya object show an S-shaped high uncertainty area for a, e and ω, respectively Fig. 5.A, Fig. 5.B and Fig. 5.E. Comparing the S-area just obtained with that of the GTO, despite the similar shape of the orbit, in this case the S is

sharper and the average uncertainty is a bit higher. These effects are probably due to the fact that the orbit is commensurable with the Earth period and the higher inclination of the Molniya orbit reduces the distances of the orbital plane from the observer position. As for the GEO and GTO case, these results show also the diagonal line for tracklets separated by 180° of true anomaly typical of the observer always outside the orbital plane.

Looking now at Fig. 5.C and Fig. 5.D, it is interesting to notice how the different position of the perigee in the space produces a shift of the horizontal low uncertainty lines. In particular, for the GTO case these lines have positions $v_1 = 90°$ and $v_1 = 270°$ for the inclination and, although not clearly visible, $v_1 = 0°$ and $v_1 = 180°$ for the RAAN; for the Molniya case is vice versa. This is due to the fact that $\omega = 270°$, then the line of the nodes coincides with the line of the semi latus rectum, while the apogee and the perigee are at the maximum angular distance from the equatorial plane. In these figures we see also high uncertainty diagonal lines for tracklets separated by 180° or 360° in true anomaly. Finally, it is important to remark two features which are visible in Fig. 5.C and Fig. 5.D: one for the inclination and one for the RAAN. Regarding i, it is interesting to notice the presence of an S-shaped low uncertainty area coincident with half a period separation between tracklets. This is probably due to the orientation of the orbit in the space. Being the apogee and the perigee the furthest points from the equatorial plane, at least one of the two tracklets which are separated in time by half a period is far enough from the this plane to clearly determine the inclination of the orbit. For the same reason the highest uncertainty areas for Ω are occurring for tracklets close to the apogee separated by one orbital period.

IV.III Influence of the second observer

The results showed until now are obtained considering a single observer. The next step of this study will be the evaluation of the effects on the uncertainty maps given by a second observer which is observing the target object precisely at the same time as the first observer. Also in this case the simulations are carried out in order to scan all possible combinations of tracklets in the same way as described in the paragraph III. The only difference is that for this study two series of observations per observer, acquired at the same time, are used in the orbit determination process.

To perform this study the following orbital parameters are used: $a = 42164.173$ km, $e = 0.5, i = 60°, \Omega = 0°, \omega = 0°$ and $T_{osc} = 1^{st}$ observation. Two equatorial observers symmetrical to the Greenwich meridian are used, whose geodetic coordinates are: for the first Lat. 0°, Long. 45° West and Alt. 900 m; while for the second Lat. 0°, Long. 45° East and Alt. 900 m.
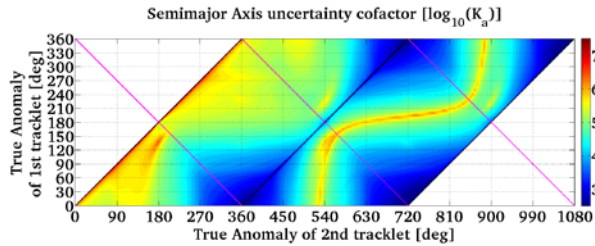
Fig. 6.A Semi-major axis uncertainty map with 2 observers.
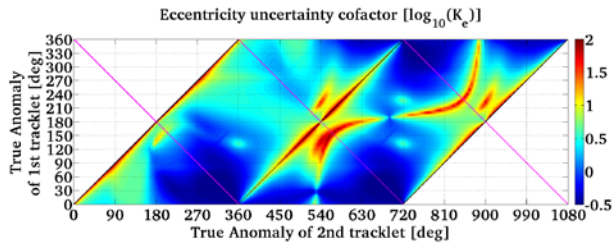
Fig. 6.B Eccentricity uncertainty map with 2 observers.
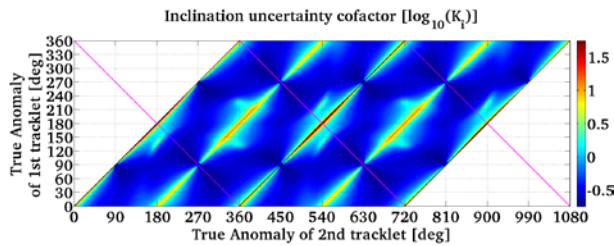
Fig. 6.C Inclination uncertainty map with 2 observers.
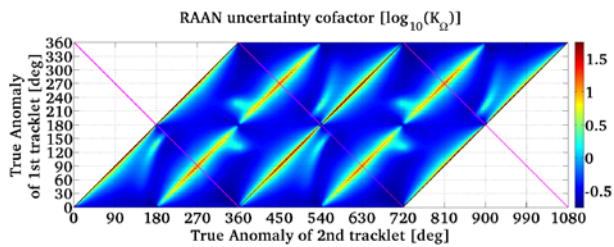
Fig. 6.D RAAN uncertainty map with 2 observers.
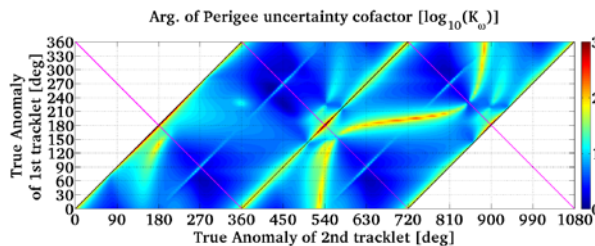
Fig. 6.E Argument of perigee uncertainty map with 2 observers.
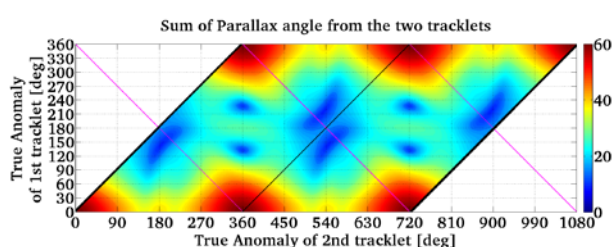
Fig. 6.F Sum of parallax angles map with 2 observers.

As one can see from Fig. 6.A, Fig. 6.B and Fig. 6.E which show respectively the uncertainty maps for a, e and ω the typical features are still present. In particular it is still possible to see the effect of the time distance between the two tracklets, in fact the maps show different features for the 1st and the 2nd orbital revolution and the average error is decreasing while the time distance is increasing. The S-shaped high uncertainty area is still present, as well as the high uncertainty diagonal line for tracklets separated by 180° and 360° in true anomaly for i and Ω, see respectively Fig. 6.C and Fig. 6.D. However, some differences can be noticed w.r.t. the case of a single observer: first, the average uncertainty values are lower due to the higher number of observations, second some new features are appearing like the high uncertainty spots close to the S-area for a, e and ω or close to the diagonal line of tracklets separated by 180° for i and Ω. The main improvement given by a second observer is given by the fact that, knowing the observers position and the directions to the target object, it is always possible to estimate the distance of the object from the observers and also its geocentric position. The quality of the estimation of such distances is proportional to the parallax angle given by the pointing directions of the observers to the object position, the smaller this angle will be the less accurate will be the distance estimation. The correspondence between the high uncertainty spots and the low parallax values is confirmed by Fig. 6.F which represents the sum of the parallax angles obtained for the first and for the second tracklets.

The most important result obtained by the introduction of the second observer is given by the capability to estimate the distances. At the same time this improvement can be reduced by the dependency of the accuracy of the estimated parameters on the parallax of the observations. This quantity is of course dependent on the relative position between observers and object. To highlight this effect, the results of a second simulation are reported in Fig. 7.A, Fig. 7.B and Fig. 7.C. These results are obtained with the same scenario previously utilized, but changing the inclination of the orbit to make it equatorial ($i = 0.1°$). Only the maps that showed significant changes are reported, namely those of a and e. As one can see, instead of high uncertainty spots on the map, in this case some new features appeared which are intersecting the nominal S-area. It is evident the correspondence between these new features with those regarding the parallax angles visible in Fig. 7.C.
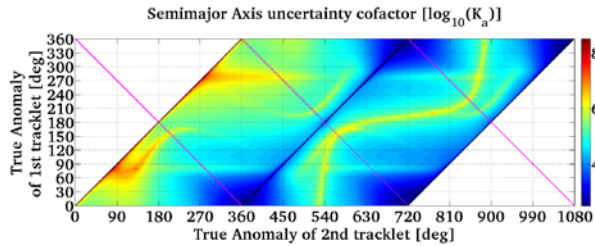
Fig. 7.A Semi-major axis uncertainty map for an equatorial geosynchronous orbit with 2 observers.
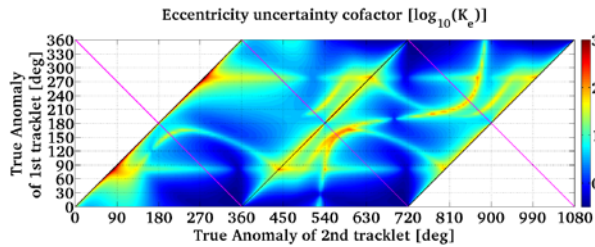
Fig. 7.B Eccentricity uncertainty map for an equatorial geosynchronous orbit with 2 observers.
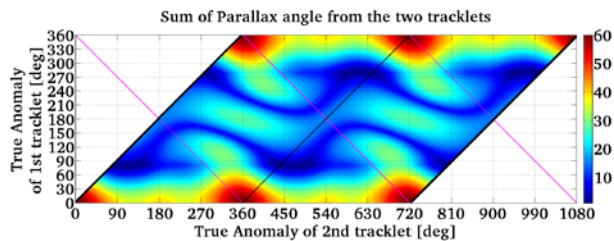
Fig. 7.C Sum of parallax angles map for an equatorial geosynchronous orbit with 2 observers.

IV.IV Third tracklet

The last results are obtained using three tracklets in the simulation of our orbit determination problem. The scenario used consists in a geosynchronous eccentric orbit with a single observer on the Earth's surface. The Zimmerwald observatory is used as the observer position while the used orbital parameters are: $a = 42164.173$ km, $e = 0.5, i = 60°, \Omega = 8°, \omega = 180°$ and $T_{osc} = 1^{st}$ observation. For this simulation the time distance between the 1st and the 2nd tracklet is kept constant to 2 hours, while the distance of the 3rd one is varying from 10 seconds up to two orbital revolutions. It was decided to set up the scenario in this way to simulate the results of a survey with the first two tracklets and then to study how the accuracy of the estimated parameters is influenced by the position of a first follow-up (3rd tracklet). As for the other cases, the observer position at the epoch of the first observation is kept constant while all the other positions (respectively for the remaining observations of the 1st tracklet and those for the 2nd and the 3rd) are determined consistently with the Earth rotation rate and the time distance from the just mentioned observation epoch. Also in this case, the simulation is performed in order to analyse all possible combinations of tracklets positions.
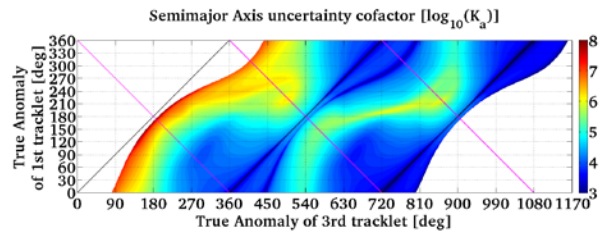
Fig. 8.A Semi-major axis uncertainty map with 3 tracklets.
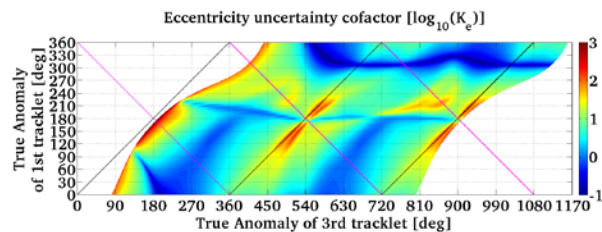
Fig. 8.B Eccentricity uncertainty map with 3 tracklets.
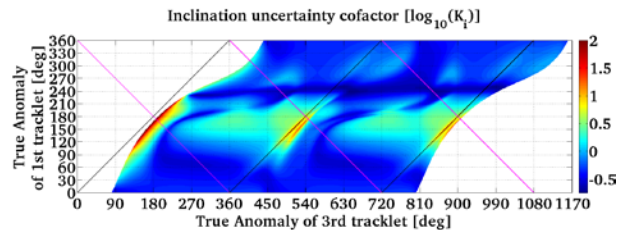
Fig. 8.C Inclination uncertainty map with 3 tracklets.
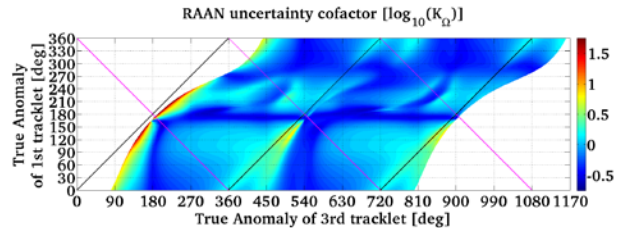
Fig. 8.D RAAN uncertainty map with 3 tracklets.
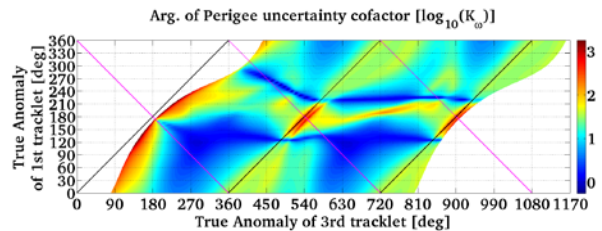
Fig. 8.E Argument of perigee uncertainty map with 3 tracklets.

As usual, the position of the 1st tracklet is represented in the y-axis while in the x-axis the position of the 3rd is shown. From these maps it is possible to see also the position of the 2nd tracklet, in particular it is roughly coincident with the first visible position of the third tracklet, this because the minimum time distance between the latter two is 10 seconds. Fig. 8.A shows the

uncertainty map obtained for the semi-major axis. As one can see the use of a third tracklet strongly reduces the average uncertainty values in comparison to those obtained for the case using only two tracklets. Despite that, as for the previous cases, the uncertainty tends to decrease with the increase of the time distance between tracklets; also the S-area is still visible but strongly reduced consistently to the higher number of observations and to the fact that the observer is always outside of the orbital plane. The part of the map where the S-area is sharper coincides with the case where the positions of the first two tracklets are close to the apogee because the slower is the object the shorter is the arc between the first two tracklets. It is still possible to see the minimum uncertainty diagonal line coincident with one period separation between first and third tracklet. It is interesting to notice that also another minimum line is appearing in this map and it coincides with the orbital period distance of the third tracklet from the second.

Looking at Fig. 8.B and Fig. 8.E, as in the case of semi-major axis, it is still possible to distinguish the residuals of the classical S-area of half a period distance between observations and at the same time, the features which in the map of a are minima regions, in the map of e and ω are high uncertainty regions. This because when the third tracklet is coincident with one of the first two one loses some useful information for the determination of e and ω. In Fig. 8.B, two horizontal lines of minimum uncertainty appeared for positions of the first two tracklets which are symmetrical w.r.t. the line of the apsides.

Finally, looking at the maps obtained for i and Ω (respectively Fig. 8.C and Fig. 8.D), it is possible to see how for positions of the 3rd tracklet which are coincident with one of the previous two there is a loss of information which produces high uncertainty values. This loss is even more evident, in the inclination map, for tracklets whose positions are close to the apogee; these positions are, in fact, coincident with the lines of the nodes. Both maps show two horizontal lines of minimum uncertainty, these appear when either the first or the second tracklet is at the maximum angular distance from the line of the nodes (for i) or is on the line of the nodes (for Ω).

V. CONCLUSION AND FUTURE WORKS

The orbit determination/improvement process is a fundamental step of the space debris research. Due to the high number of object and the limitations of the instruments used for the measurements acquisition, it is necessary to optimize the use of the time available for observations, being it for surveys or follow-ups. This paper presented the results obtained by a study whose aim was to highlight the dependency of the accuracy of the parameters, estimated during an orbit determination, on the object-observer relative geometry. The study was performed by analysing the output covariance matrix obtained from the simulation of a LSQ adjustment process. The results of the simulations allowed us to create an uncertainty map for each estimated parameter, which shows the uncertainties as a function of the relative positions of the observation series. At the beginning, a "standard" orbit is used to evaluate the influence of the observer position; successively the effects of each orbital parameter are analysed. These first simulations allowed us to understand the main factors which are influencing the accuracy of the results of an orbit determination like: the time interval between tracklets, the inclination of the orbit, the angular distance from the line of the nodes and from the lines of the apsides, the influence of the observer position w.r.t the orbital plane, the distance of the object in terms of Earth's parallax, the arc-length of the tracklet and the ratio between orbital period and sidereal day. Successively, two more complex scenarios are analysed. First the case of two observers which are observing synchronously the same object is studied; second, the case of three series of observations is analysed. The main advantages given by the second observer can be summarized in the capability to estimate distances knowing the two observers positions and the target direction from the observer; at the same time these results showed also their strong dependency from the parallax angle given by the pointing directions of the observers to the object position. To be more precise, the smaller is the parallax angle the higher is the uncertainty obtained for the estimated parameters. The analysis of the case with three series of observations showed mainly that the main effects, noticed in the case of the two tracklets, are amplified by the relative combinations among the three tracklets.

The proposed method can be also used to study more general scenarios and can be applied also to different orbital regimes. For example an interesting application could be to use two or more observers which are not observing at the same time in order to optimize also the observation strategy of a network of telescopes or to simply evaluate the improvements given by a second observer for a Low Earth Orbit object. Finally this method can be used to study what kind of improvement can be obtained by another kind of observable, like ranges, or even by merging different observables in the orbit determination problem (e.g. angular measurement and ranges).

VI. ACKNOWLEDGMENT

1 Clean Space. *ESA* [Online] May 2015. http://www.esa.int/Our_Activities/Space_Engineering_Technology/Clean_Space/How_many_space_debris_objects_ are currently_in_orbit.

2 United Nations, Office for Outer Space Affairs. *Technical Report on Space Debris.* A/AC.105/720, United Nations Publication Sales No. E.99.I.17, ISBN 92-1-100813-1, United Nations, New York, USA, 1999.

3 Schildknecht, T., Herzog, J., Vananti, A., Ploner, M., Fletcher, E. Coordinated Optical GEO Survey for European SSA Precursor Services. Proceedings of *AMOS Conference*, Maui, Hawaii, 2013.

4 Schildknechtm T., Vananti, A., Hinze, A., Herzog, J., Ploner, M. Long-term evolution of high area-to-mass ratio objects in different orbital regions. Proceedings of *AMOS Conference*, Maui, Hawaii, 2012.

5 Schildknecht, T., Herzog, J., Hinze, A., Vananti, A., Ploner, M. AIUB efforts to survey, track, and characterize small-size objects at high altitudes. Proceedings of *DLRK Conference*, Berlin, Germany, 2012.

6 Silha, J., Schildknecht, T., Hinze, A., Vananti, A. Additional optical surveys for space debris on highly eccentric and inclined MEO orbits. Proceedings of *65th International Astronautical Congress*, Toronto, Canada, 2014.

7 Beutler, G. *Methods of Celestial Mechanics, Vol I/II.* Springer-Verlag, ISBN:978-3540407492/ISBN:978-3540407508, Berlin, Germany, 2005.

8 Vallado, D. A. *Fundamentals of Astrodynamics and Applications – 4th Ed.* Microcosm Press, ISBN:978-1881883180, March 2013.